FERMILAB-PUB-14-345-TD

Giant two-phonon Raman scattering from nanoscale NbC precipitates in Nb

C. Cao[1,2], R. Tao[3], D.C. Ford[2], R. Klie[3], T. Proslier[2], L. Cooley[4], A. Dzyuba[4], P. Zapol[2],

M. Warren[1] , H. Lind[5] and J. F. Zasadzinski[1,2, †]

[1] *Physics Department, Illinois Institute of Technology, Chicago, Illinois 60616, USA*

[2] *Material Science Division, Argonne National Laboratory, Argonne, Illinois 60439, USA*

[3] *Physics Department, University of Illinois at Chicago, Chicago, Illinois, 60607, USA*

[4] *Superconducting Materials Department, Technical Division,Fermi National Accelerator Laboratory, Batavia, Illinois, 60510 USA*

[5] *Department of Physics, Chemistry and Biology (IFM), Linköping University, SE-581 83 Linköping, Sweden*

Received on September 19, 2014

ABSTRACT

High purity niobium (Nb), subjected to the processing methods used in the fabrication of superconducting RF cavities, displays micron-sized surface patches containing excess carbon. High-resolution transmission electron microscopy and electron energy-loss spectroscopy measurements are presented which reveal the presence of nanoscale NbC coherent precipitates in such regions. Raman backscatter spectroscopy on similar surface regions exhibit spectra consistent with the literature results on bulk NbC but with

significantly enhanced two-phonon scattering. The unprecedented strength and sharpness of the two-phonon signal has allowed a direct comparison to *ab-initio* calculations of phonon dispersion curves, where it is shown that the two-phonon peaks are linked directly to phonon anomalies arising from strong electron-phonon interaction. The exact origin of the stronger two-phonon response is not known at present but it suggests the possibility of enhanced electron-phonon coupling in transition metal carbides under strain found in NbC inclusions or at their interfaces with Nb metal. Preliminary tunneling studies using a point contact method show some energy gaps larger than expected for bulk NbC.

† Corresponding author zasadzinski@iit.edu

PACS: 63.20.D-, *74.25.nd,* 68.35.Ja, *63.20.dk*

I. INTRODUCTION

Superconducting transition metal nitrides and carbides have been intensely studied due to their physical properties of high hardness and chemical stability as well as transition temperatures, T_c, above that of Nb [1]. Potential devices utilizing thin films of transition metal compounds, which might replace those currently using Nb, continue to draw attention [2-5]. Some transition metal carbides (e.g. NbC, TaC) are of particular interest as neutron scattering has revealed several pronounced anomalies (dips) in the phonon dispersions, at particular $\boldsymbol{q}$ vectors, that are due to the renormalization effects of strong electron-phonon interaction [6], usually linked to nesting features of the Fermi

surface [7, 8]. Such compounds serve as a natural testing ground for *ab initio* calculations of the electronic band structure, lattice dynamics, electron-phonon (e-ph) interaction and superconducting T_c and thus remain an active area of investigation [9-11]. New theoretical methods incorporating correlation effects are also being applied, leading to renewed interest in classic, e-ph mediated superconductivity, especially for tailored, functional materials [12].

During the early 1980's it was discovered that Raman spectroscopy was providing important insights into the e-ph interaction and superconductivity. Two-phonon Raman scattering, a higher-order and therefore generally weaker process, was found to be strong in transition metal compounds with relatively high T_c (e.g. NbC, TaC) but absent in low T_c materials, (e.g. HfC) [13]. Subsequent theoretical investigations of the Raman matrix element showed that peaks in two-phonon Raman should originate in the same electronic scattering processes that give rise to phonon renormalization effects [14] and are related to the electron-phonon spectral function, $\alpha^2F(w)$, measured by tunneling [15, 16]. A correlation between two-phonon Raman and phonon anomalies has also been suggested for NbN [17].

Here we show that the two-phonon Raman scattering from NbC can be unusually strong and sharp, much stronger than previously observed on bulk samples. The NbC studied here is in the form of nanoscale inclusions near the surface of strained and chemically-polished Nb, and high resolution transmission electron microscopy (TEM) shows that these inclusions are coherent with the Nb lattice. The unprecedented strength and sharpness of the two-phonon Raman has now allowed a direct comparison to calculated phonon dispersions of NbC under compressive strain, showing directly that the

two-phonon peaks correspond to the regions of phonon anomalies. We also present a computational model of the interface between Nb and NbC that accounts for a close lattice match between the two materials. Finally, we present preliminary point contact tunneling spectroscopy data from these NbC regions where superconducting gaps are found that are larger than those found on the pure Nb regions and in some cases larger than expected for bulk NbC.

II. IDENTIFICATION OF NIOBIUM CARBIDE INCLUSIONS BY TEM AND EELS

The specimens investigated here were discovered by serendipity. NbC is an occasional unwanted by-product of preparing superconducting radio-frequency (SRF) cavities from high-purity Nb metal by an empirical recipe that includes deep-drawing, acid polishing, and annealing. Materials science investigations of either cut-outs of tested SRF cavities at failure locations [18, 19], or from pristine Nb plates, foils, etc. prepared like SRF cavities [20], have found that such processing of Nb can lead to micron-sized surface patches, easily seen as dark spots under an optical microscope, that contain high amounts of carbon as revealed by Raman and scanning electron microcopy (SEM) [18]. While the mechanism of NbC formation is still under investigation, combinations of strain and annealing reproducibly produced carbon and NbC clusters, more readily so in samples that received chemical polish. The affinity of carbon for linear defects [21, 22] might be important for this process. The present study is novel in that high-resolution TEM and

electron energy loss spectroscopy (EELS) have been coupled to study these excess C patches.

The Nb host material is described in [20]. The particular specimen came from a high purity, cavity-grade (< 20 ppm carbon by mass) rectangular rod ($2 \times 2 \times 75$ mm^3) cut by discharge machining from a polycrystalline plate (grain size >45 μm) in a recrystallized state [23], and strained to 56% total elongation by a tensile stress test machine. The ends of the rod extended past the grip points, and remained unaffected by tensile strain. The entire rod was electropolished to remove 180 μm of metal as in [24], ultrasonically cleaned with a hydrocarbon-removing detergent, rinsed in ultra-pure water, and subsequently annealed at 800 °C in high vacuum for 2 hours. Such processing re-traces the steps used in SRF cavity construction [20]. Two pieces of the rod, one from the middle strained region, sample #1, and one from the end, sample #2, were studied. These samples were scanned by SEM, and surface patches which showed high C content were cut out by focused Ga-ion beam (FEI Helios Nanolab 600) for TEM analysis. These TEM/EELS analyses was conducted in an aberration-corrected cold-field emission instrument (JEOL ARM200CF) at the University of Illinois at Chicago.

Figure 1(a) shows an aberration-corrected STEM annular dark field (ADF) image from the surface of sample #2. A thin surface layer ~ 90 nm thick is observed which displays a clear difference in contrast. Both low-loss (Fig. 1(c)) and core-loss (Fig. 1 (d)) EELS show different spectra in the two regions. In particular, a low energy feature near 10 eV, characteristic of bulk Nb, is absent in the surface layer. The carbon content in the surface region is approximately 50% and EEL spectra indicate it is ordered NbC. Figure 1(a) also shows an atomic-resolution ADF image (Nb atoms only) of the boundary

between the two different regions as indicated by the broken line. The atomic plane of bcc Nb is observed with no apparent change in lattice parameter crossing the boundary. Thus, the fcc NbC is a coherent precipitate, commensurate with the bcc Nb matrix.

In Fig. 2(a) is shown an annular bright field (ABF) image from the surface of sample #1. Three inclusions are observed with characteristic dimensions from ~60 nm (middle) to ~1mm (top). An expanded view of the middle inclusion is shown in Fig. 2(b) showing a clear image contrast. A core-loss EEL spectrum image is taken from the region indicated by the green box and the corresponding integrated intensities for the Nb M-edge, the C K-edge and the O K-edge are also shown. Figure 2(c) shows an atomic-resolution ADF image of the interface between the inclusion and the Nb bulk, again with no visible change in crystal structure crossing the boundary. The EEL spectra from these two regions are shown in Fig. 2 (d) and 2(e). Here, the red curve is characteristic of pure Nb whereas the black curve shows peaks characteristic of NbC including the sharp C peak near 288 eV.

The conclusion from the STEM studies is that NbC may have resulted from residues of sheet processing, electropolishing, annealing, and perhaps other artifacts of careful handling, with distinct precipitates appearing in regions with added tensile strain. This is consistent with studies of NbZrC alloys with low concentrations of Zr (~1%) and C (~0.4%), which show that, with annealing only, NbC precipitates form throughout the Nb matrix that are very stable [25]. However, the results here show that the NbC near the surface is coherent with the host Nb. Friction with rollers, and injection of hydrogen

during electropolishing, are known sources of strain at the niobium surface that are not present in the bulk.

III. RAMAN SPECTRA OF NIOBIUM CARBIDE INCLUSIONS

Raman spectroscopy was performed on many types of as-processed Nb including cavity cut- outs, strained/annealed foils, bars, and samples #1, #2 discussed above. All Raman measurements were done using a Renishaw, inVia, Raman microscope with a 785 nm laser source, 30 s exposure time, 100% laser power [27 mW], and a 50X objective. The laser spot size is ~3 mm diameter, ideal for examining these rough surface patches which have lateral dimensions from 10-100 mm. Previous Raman studies of these patches revealed spectral peaks identified as amorphous C and chain-type hydrocarbons [18].

In Fig. 3(c) are shown a set of Raman spectra from regions of a processed Nb sample that exhibited a number of surface patches, examples of which are shown in the photographs in Fig. 3(a). This particular Nb sample A was processed at JLab according to the following procedures: spark cut from a large grained Nb plate, buffered chemical polish, electropolish (EP), vacuum anneal at 600°C for 10 hours, and a final EP. There appear to be three main peaks near 12 THz although the highest frequency peak is a doublet indicating two modes close in frequency. These peaks are highly reproducible and are observed in a variety of patches on this sample. Other processed Nb samples showed similar spectra. Examples are shown in the bottom panel of Fig. 3(c) from a

"hotspot" cut-out of a Nb cavity that exhibited a medium field Q drop (see [26] for details). Some patches on various Nb samples displayed relatively broad Raman peaks due to amorphous carbon only [18]. These peaks are also seen in the spectra presented in Fig. 3(c) but at higher wavenumber and not shown. The presence of excess carbon suggested the sharper peaks might be due to an ordered Nb carbide phase and this is confirmed by comparison to published Raman spectra on bulk NbC [13] as shown in Fig. 3(b) where a particular spectrum from this work is presented for comparison.

The band of peaks near 6 THz are similar in location and shape to the acoustic phonon DOS observed obtained from neutron scattering [27] and observed in earlier Raman studies of bulk NbC [13, 27]. However, the Raman band here is shifted to higher frequencies suggesting a volume compression of our precipitates, as argued before [11]. The optical phonons centered near 18 THz also appear shifted to higher frequencies compared to the neutron DOS. It should be noted that first order Raman is normally forbidden in NbC and thus the observation of the full phonon DOS is indicative of disorder-induced first order Raman suggesting C vacancies are responsible, as found in bulk NbC [13].

The sharp peaks of the present study near 12 THz show good agreement with a similar band in bulk NbC which has been identified as two-phonon Raman arising from acoustic plus acoustic, (A+A) processes [13]. In particular, a closer examination of the A+A region in bulk NbC reveals 3 subtle peaks which agree quite well with the peaks observed here. But whereas this band is a weak effect in bulk NbC it is by far the dominant feature of the present study, strongly exceeding the first order Raman signal. This is not unphysical as the first order response should be zero by symmetry and exists

only due to disorder [13]. Examination of all of the spectra of Fig. 3(c) shows that this anomalously strong two-phonon band is a characteristic feature of these NbC precipitates. Furthermore, the sharpness of the A+A peaks consistently reveal that highest frequency peak is really a doublet indicating two distinct peaks. The highest band of modes near 24 THz is also in good agreement with bulk NbC and has been identified as acoustic plus optical, A+O two-phonon channel [13]. For this band there does not appear to be the strong enhancement but nevertheless we observe three distinct peaks, characteristic of the LO and TO phonon bands, whereas the bulk NbC data [13] shows a broad band without much structure.

IV. FIRST PRINCIPLES CALCULATIONS OF PHONON DISPERSIONS AND DOS

It is worthwhile to consider in more detail how fcc NbC (a = 4.47 Å) might be commensurate with bcc Nb (a = 3.30 Å). We consider two possible arrangements. The first possibility is that the close packing (111) plane of the NbC is parallel to the (110) plane of Nb. In Fig. 1(b) are shown the atomic arrangements and interatomic distances for Nb atoms in these planes based on bulk lattice parameters. Considering a five-atom, body centered rectangle in the (111) plane in NbC, this can be made commensurate with a similar rectangle in (110) Nb by an elongation of the short side from 3.16 Å to 3.30 Å and a compression of the long side from 5.47 Å to 4.67 Å leading to an overall area compression ratio of 0.89. For the volume, if we force the d-spacing of the (111) planes of NbC to match that of the (110) planes of Nb there is a further contraction leading to an

overall volume compression ratio of 0.81. But this assumes the intrinsic lattice constant for the NbC is the bulk, stoichiometric value. While we do not have independent, exact measurements of the carbon concentration, there are likely C vacancies, which will reduce the lattice constant. Some NbC inclusions in steels [28] have been found with lattice constant a = 4.36 Å, and using this value increases the volume compression ratio of our precipitates to 0.87. The principal conclusion in this model is that the coherent, nanoscale NbC precipitate is under anisotropic, but overall compressive stress.

The second possibility is that the (110) plane of NbC is parallel to the (110) plane of Nb. This arrangement is commensurate under a relatively small tensile strain in NbC of 1.04, which is in-plane isotropic, resulting in elongation of the short side from 3.16 to 3.30 Å and of the long side from 4.47 to 4.67 Å. In this model there is no symmetry breaking of the fcc NbC. The corresponding Nb rectangle in NbC does not have a Nb atom in the center as compared to the Nb rectangle shown in Fig. 1(b), however, a view of the interface from a complementary (110) direction provides a close match to the TEM image in Fig. 1(a) because the out-of-plane Nb atoms can also be seen in the center of the rectangle as shown in Fig. 1(b). The following investigation of vibrational properties provides insight into comparison of these two models.

Phonon dispersion curves for NbC in a B1 NaCl structure were generated by density functional theory calculations performed within the Quantum Espresso package [29] using plane waves and ultrasoft pseudopotentials [30] along with density functional perturbation theory [31] and harmonic approximation for the phonon calculations. Exchange-correlation effects were treated using generalized gradient approximation according to Perdew-

Burke-Ernzerhof [32]. The k-mesh used was a 24x24x24 Monkhorst-Pack grid and the q-mesh for the phonons was an 8x8x8 grid. Occupation numbers were determined using the Methfessel-Paxton scheme with a broadening parameter σ=0.025 Ry and a plane wave energy cutoff of 40 Ry was also used.

The unusual strength and sharpness of the two-phonon Raman has stimulated us to examine the relationship between these peaks and phonon anomalies in dispersion curves. Direct comparison to the calculated bulk NbC phonon dispersion curves showed modest overall agreement with the two-phonon Raman, however, given the shift of the acoustic branch DOS, and the likely compression of the coherent precipitates, we compared the data to NbC phonon dispersions under a uniform volume compression of 0.88. As shown in the bottom panel of Fig. 3(b) the shift of the calculated acoustic DOS with 0.88 volume is in much better agreement with measured first order Raman spectrum. Using this compression, very good overall agreement between two-phonon Raman and phonon dispersions was found as shown in Fig. 4. Each peak of the two-phonon Raman (with frequency axis divided by 2) corresponds to regions of phonon anomalies. In particular the doublet near 7 THz appears to be due to the close frequencies of the strong phonon dips along the G-X and G-K directions as well as the L point in the Brillouin zone. The two lower peaks in the range 5-6 THz also correlate well with regions of phonon dips. A small peak near 8 THz tentatively corresponds to the dip at the W point. In effect, all of the regions where strong phonon renormalization is occurring correspond to a two-phonon Raman peak. To our knowledge, such a correlation has not been achieved before on any superconducting transition metal compound.

On the other hand, we approximated a strongly anisotropic in-plane deformation, which potentially breaks symmetry and might result in additional Raman peaks, by a uniform isotropic compression. Also, such a compression results in a shift of optical phonon frequencies upwards (not shown), which is not observed in experimental spectra. Therefore, we have also investigated vibrational properties for our second structural model, Nb(110)/NbC(110) interface, which has a smaller and uniform in-plane deformation.

We modeled the interface structure using a six layer thick slab of bcc Nb cut along the (110) plane matched to a four layer thick slab of fcc NbC cut along the (110) plane as shown in Fig. 1 (b), with periodic boundary conditions. Density functional theory as implemented in VASP [33] was used to optimize the geometry and density functional perturbation theory was used to calculate the force constants. Phonopy [34] was used to produce the phonon DOS, shown in Fig. 3. We also calculated the DOS for bulk Nb, bulk NbC, and bulk compressed NbC, and show them in Fig. 3(b) for comparison. The peak widths and positions of the interface model for both the acoustic and optical one-phonon regions match well with the observed Raman spectra as shown in Fig. 3(c). Both optical and acoustic regions are broadened for the interface model when compared to bulk Nb and NbC. Partial DOS in Fig. 3(c) indicate that the phonon states associated with Nb close to the interface are responsible for broadening of the acoustic one-phonon peaks. An analysis of optimized geometries indicates presence of shorter Nb-C distances at the first interface layer, which strongly correlates with the acoustic phonon states observed at higher frequencies. Decrease in symmetry is often cited as a reason of strong two-phonon Raman signal, which correlates well with our measurements in Fig. 3.

V. EVIDENCE OF AN INCREASED SUPERCONDUCTING GAP FROM POINT CONTACT TUNNELING

The origin of the strong two-phonon Raman in these NbC precipitates is not fully understood at present. One possibility is that this is the intrinsic response of NbC and bulk samples simply haven't revealed it, instead showing reduced, broadened features due possibly to surface imperfections. The bulk NbC Raman spectra were variable and sensitive to surface preparation and polishing methods [13]. The other possibility is that these precipitates are showing an enhancement of the two-phonon Raman, above that of bulk NbC. Given that the sizes of the precipitates are variable, it does not seem to be a simple size effect causing the enhancement. It might originate in the anisotropic strain that these fcc NbC inclusions are under as a result of their coherency with the host Nb matrix or in the local structures at the interfaces between Nb and NbC inclusions. Considering theoretical models [14] the two phonon strength is tied to the electron-phonon spectral function [16], $\alpha^2F(\omega)$, and there is the possibility that this spectral function may have also been enhanced in these NbC inclusions. Hence, they may even have a larger T_c than bulk NbC.

To test this possibility, tunneling measurements using a mechanical contact were initiated. Patches exhibiting NbC Raman spectra were found frequently on the sample A. A region rich in such patches, approximately 20 by 50 micron in size, was identified under Raman microscope and its location marked on the sides of the sample. We then aligned a PtIr tip on top of the region of interest and searched for tunnel junctions through

a point contact method [35]. Near stoichiometric NbC should have a superconducting T_c close to 12 K [36]. Using this value and assuming a similar strong coupling ratio, $2\Delta/kT_c$ = 3.9, as that of Nb (with Δ = 1.55 meV), an estimated Δ = 2.0 meV for the expected gap parameter of NbC is obtained. Some tunneling spectra with large energy gaps were observed as shown in Fig. 5. In general, these large gap spectra are relatively broad and exhibit a double gap feature with the small gap resembling that observed for a Nb region outside the patch, (bottom red curve of Fig. 5). The multigap feature could be interpreted as the tip covering both a NbC patch and the surrounding Nb, forming parallel junctions. However, TEM studies show that the top surface above a NbC inclusion often does not exhibit a Nb oxide layer, (e.g. Fig. 1(a)), and thus would not be expected to have a native, insulating tunnel barrier. Thus the two-gap feature may be the result of some type of proximity effect. Despite this uncertainty, single gap fits of the larger gap feature were performed and these lead to Δ values in the range of 2.1 meV to 3.3 meV among the three junctions in Fig. 5. The values at the low end would be consistent with estimates for bulk NbC, but those at the high end would suggest a local NbC phase with T_c significantly higher than 12 K and approaching 20 K.

VI. CONCLUSIONS

In summary, high purity Nb, subjected to the processing steps of strain, etching and annealing used in the fabrication of SRF cavities, consistently reveals micron sized surface regions that contain excess carbon. The new results of this study show that, in addition to amorphous C and chain-type hydrocarbons observed earlier by Raman, there

exist nanoscale precipitates of NbC at the surface. High resolution TEM reveals no observable change in lattice constant of the Nb indicating the NbC is coherent with the Nb host. These same types of excess C patches often reveal Raman backscatter spectra consistent with earlier measurements of bulk NbC but with a significantly enhanced two-phonon Raman signal. The strength and sharpness of the two-phonon spectrum has allowed a direct comparison to DFT calculations of the NbC phonon dispersions (under compressive strain), where it is shown directly that peaks in two-phonon Raman correspond to regions of phonon softening due to e-ph renormalization. Thus, theoretical notions that the two-phonon Raman strength is tied to phonon anomalies and the electron-phonon spectral function, $\alpha^2F(\omega)$, have been substantiated. An interface model for Nb/NbC also suggests presence of local vibrational modes at the interface that can give rise to sharp two-phonon Raman features. This interface model also explains the upward frequency shift of the acoustic modes and the corresponding insensitivity of the optic modes as is observed in the Raman. The origin of the strong two-phonon Raman is not fully understood at present but there is the possibility that $\alpha^2F(\omega)$ may have been enhanced in these NbC inclusions, a result supported by preliminary tunneling data. If so, then this suggests that there may be new pathways for manipulating the e-ph interaction, and raising T_c, in transition metal carbides.

ACKNOWLEDGEMENTS

The authors thank G. Ciovati of Jefferson Laboratory for supplying Nb samples used in this study. Calculations (H.L.) were performed with financial support by the SSF-project

Designed multicomponent coatings, MultiFilms and the Swedish Research Council. Calculations were carried out at the Swedish National Infrastructure for Computing (SNIC), Argonne LCRC and Argonne Center for Nanoscale Materials. The work at Argonne National Laboratory and the use of the Center for Nanoscale Materials and the Electron Microscopy center at Argonne National Laboratory were supported by the U.S. Department of Energy, Office of Science, Office of Basic Energy Sciences under contract No. DE-AC02-06CH11357. This work was also supported by the Department of Energy, Office of Science, Office of High Energy Physics, early career award to T.P.

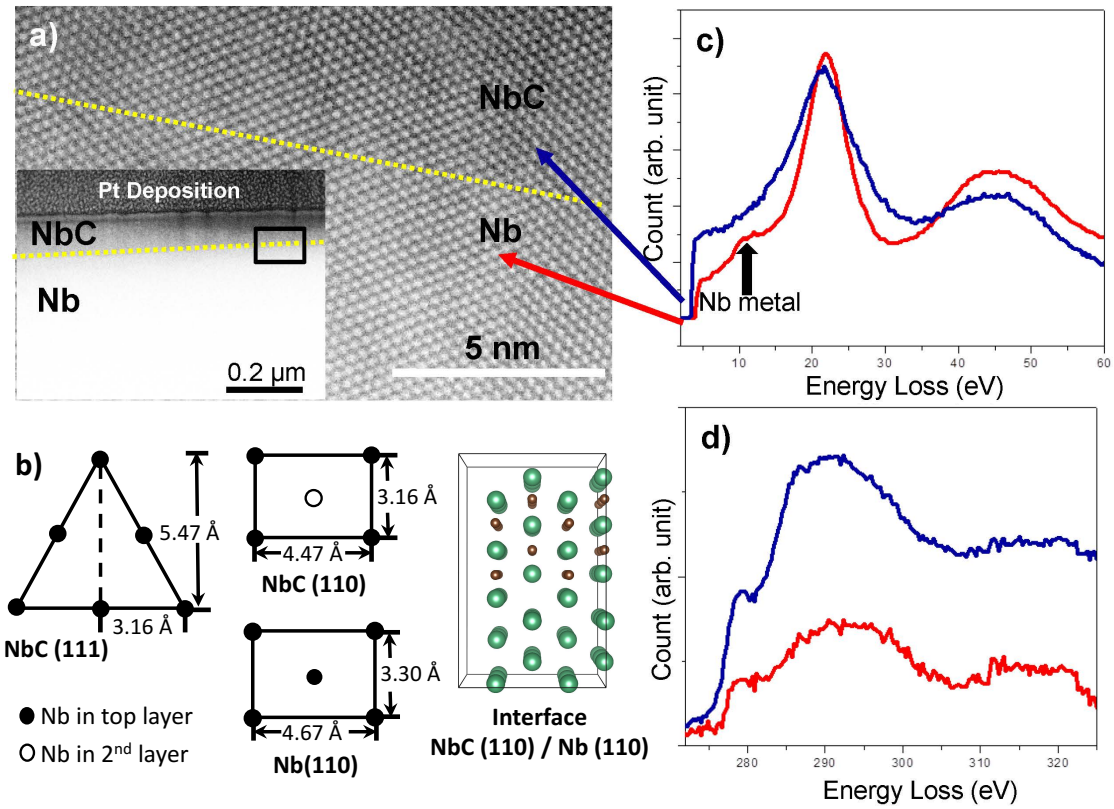

FIG. 1 (a) Inset shows an aberration-corrected STEM annular dark field image of surface of Nb rod sample #2 which shows ~ 90 nm thick region with a different contrast compared to the bulk Nb. Main panel shows atomic-resolution image of the interface between the surface inclusion and the Nb bulk, indicated by the broken line. The atomic plane of bcc Nb is observed with no evidence of any change in lattice constant across the boundary. (b) Nb atom arrangements for the (111) and (110) planes of NbC, the (110) plane of Nb, and an atomic model of the interface between NbC (110) / Nb (110). In the atomic model, Nb atoms are represented as large green spheres and C atoms are small brown spheres. (c) Low-loss EELS spectrum of Nb (red curve) and NbC (blue curve) regions. A shoulder at ~10 eV, characteristic of Nb is absent in the region near the

surface which is likely NbC. (d) Core-loss EELS spectra for Nb (red curve) and NbC (blue curve).

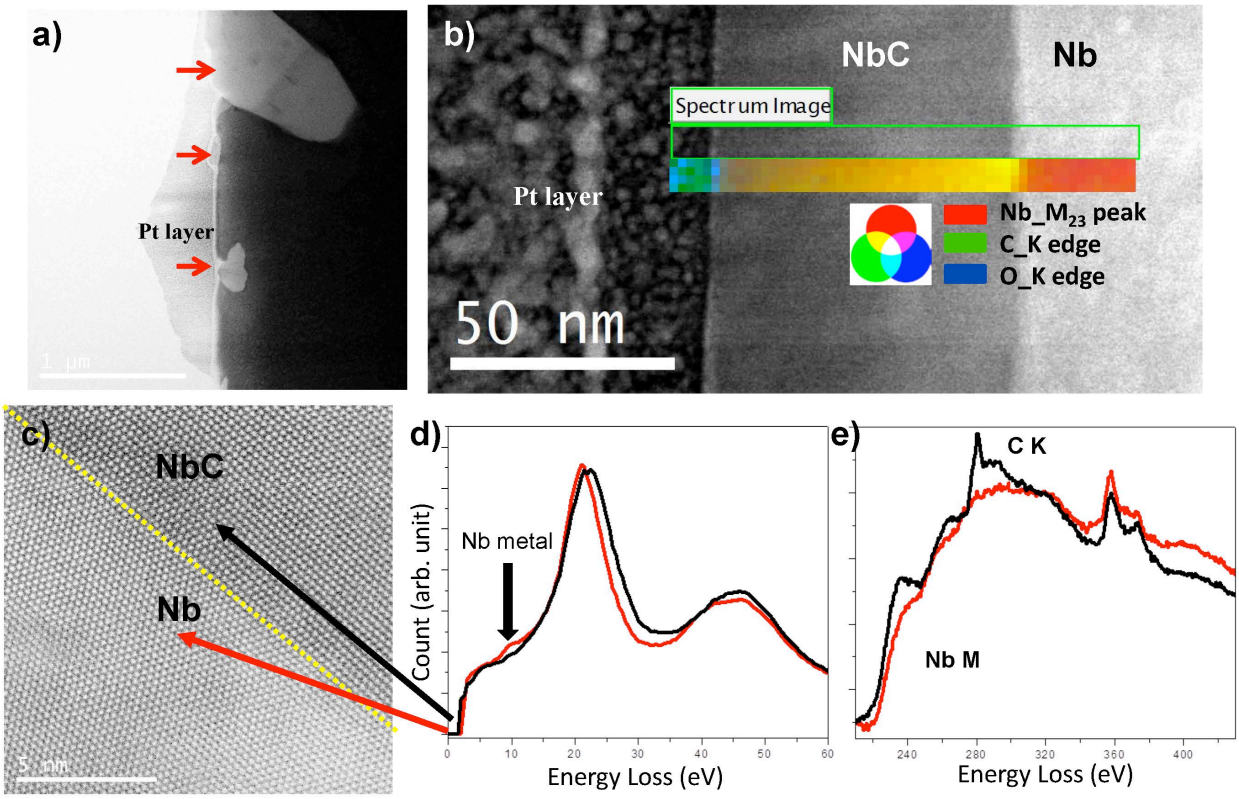

FIG. 2. (a) Annular bright field (ABF) image from sample #1. Three NbC inclusions (indicated by arrows) are observed varying in linear dimension from ~1 mm long (top) to ~60 nm across (middle). (b) ABF image of the middle inclusion with composition of the Nb bulk and the inclusion indicated by the integrated EEL spectrum intensities. (c) Atomic-resolution image of the interface between the bottom inclusion and the Nb bulk. (d-e)_ Low-loss and core-los EEL spectra from the two regions indicated in (c). The black EELS curve shows peaks consistent with NbC including the sharp C peak centered at 288 eV.

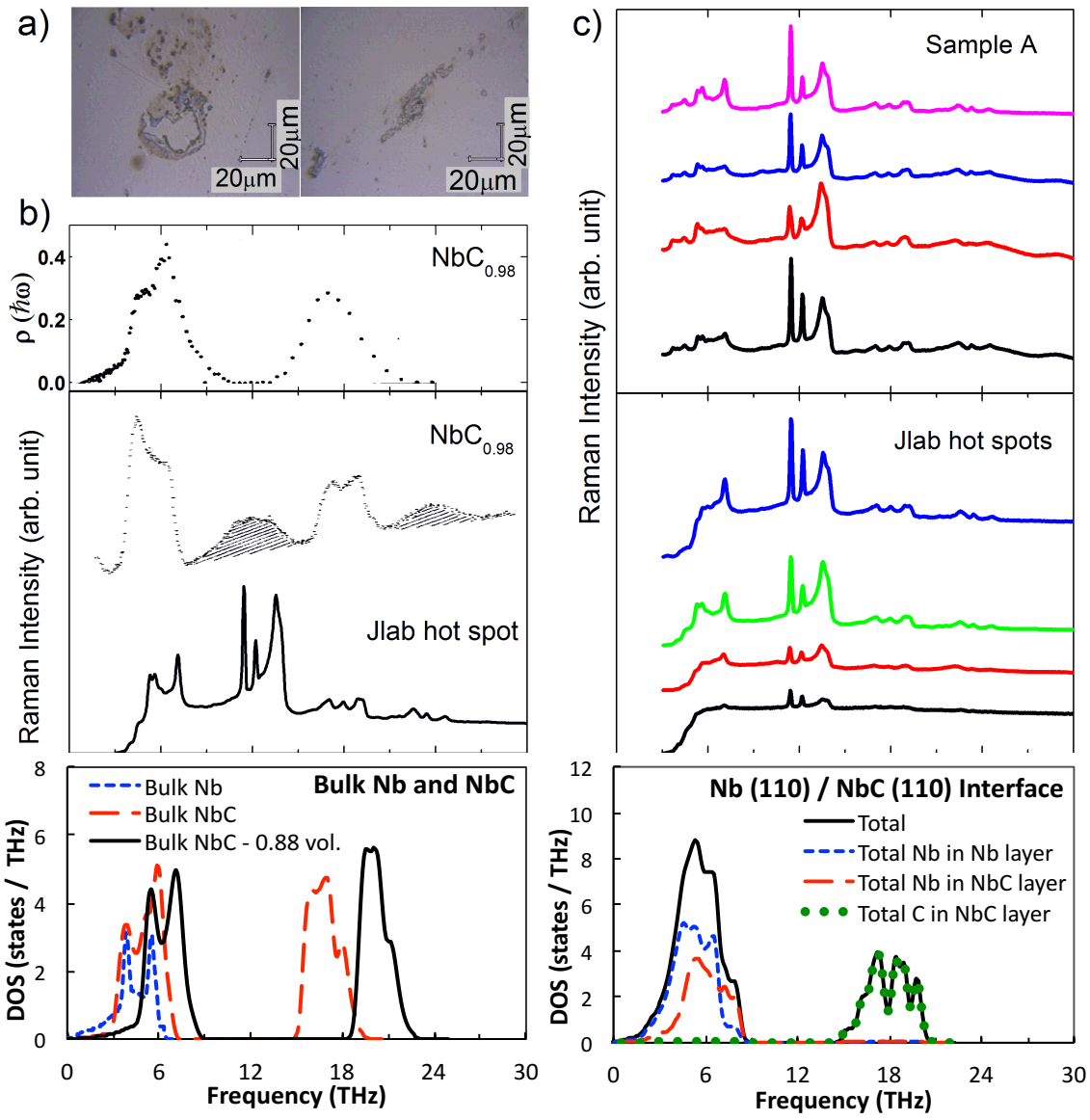

FIG. 3. Microscope camera photos of surface patches on JLab sample A (a), a representative Raman backscatter spectra shown in comparison to Raman data (ref. 13), the phonon DOS of $NbC_{0.98}$ measured from neutron scattering (ref. 26) and the phonon DOS of bulk Nb, NbC, and compressed NbC calculated using DFT (b), and representative Raman spectra from JLab sample A and cavity pieces cut out from hot spots, and total and partial phonon DOS for the Nb(110)/NbC(110) interface model calculated using DFT (c). Dashed shaded regions in (b) correspond to two-phonon A+A

near 12 THz and A+O regions near 24 THz. Raman spectra in (c) are highly reproducible and characterized by four peaks centered near 12 THz.

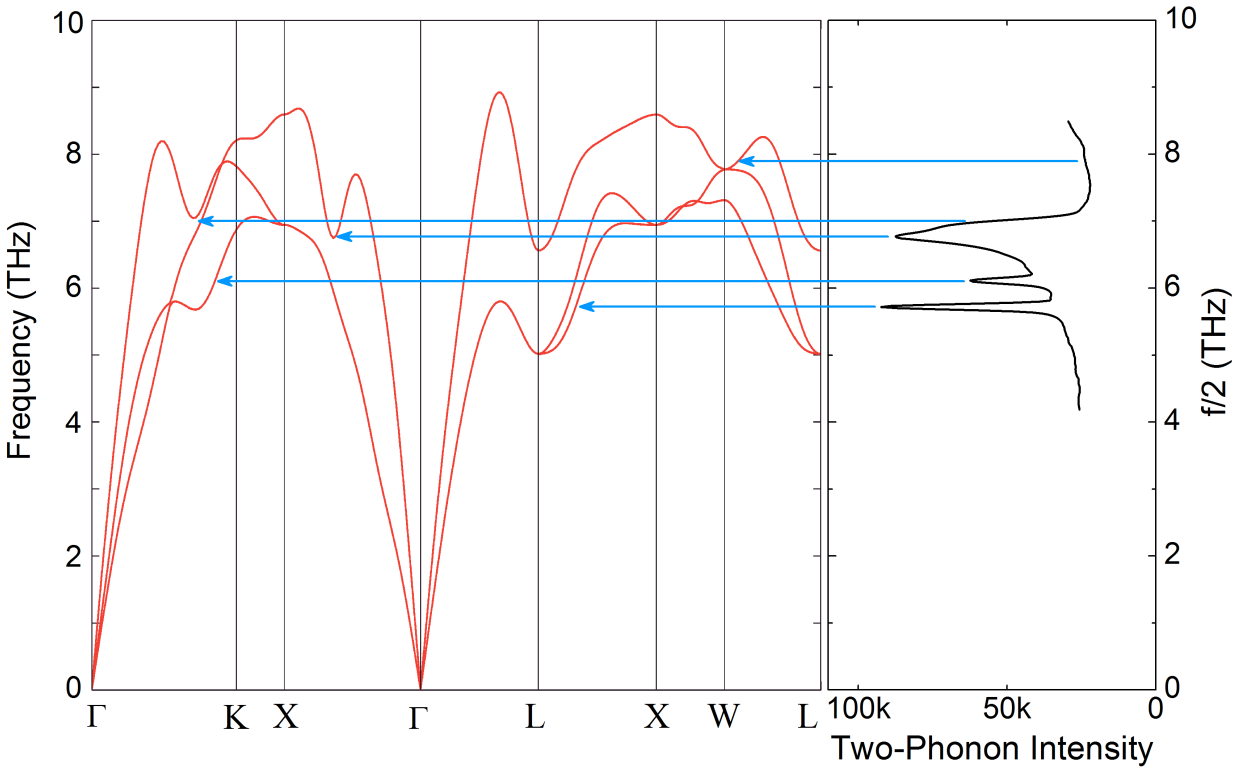

FIG. 4. Comparison of calculated phonon dispersions for NbC under uniform volume compression of 0.88 of the bulk volume to a representative two-phonon Raman spectrum from a processed Nb sample. Arrows suggest the regions of strong phonon renormalization responsible for the two-phonon peaks.

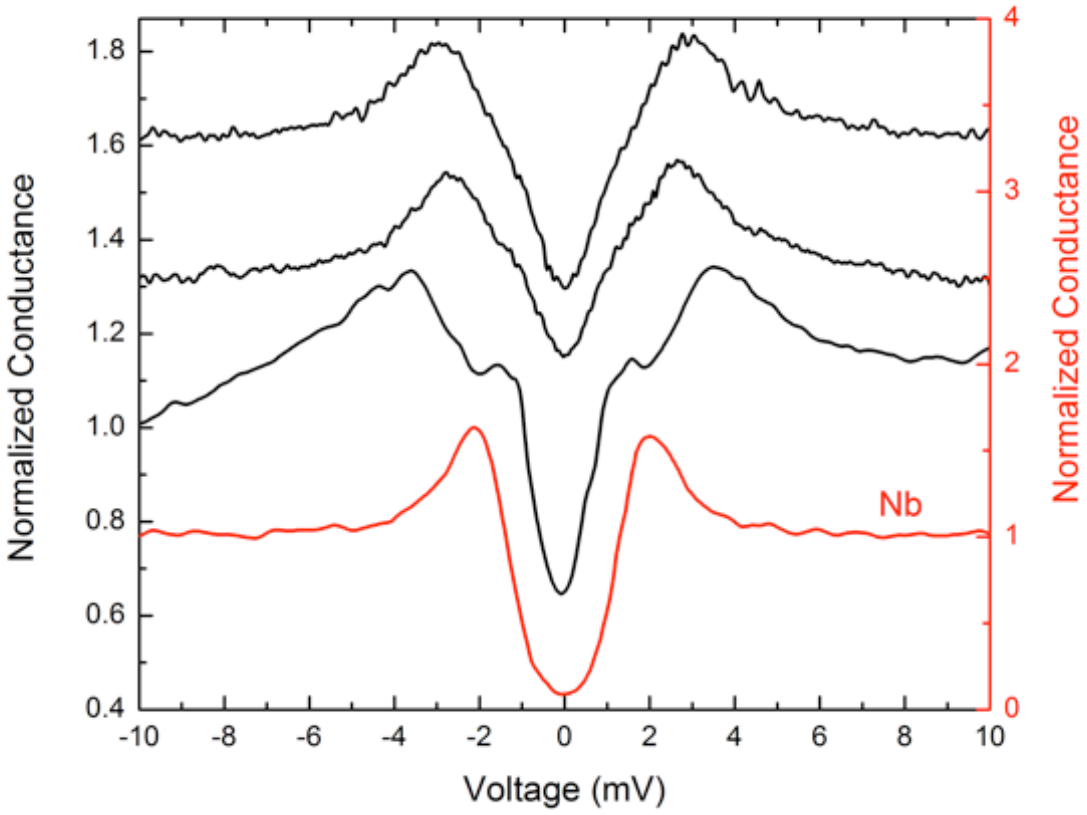

FIG. 5. Normalized tunneling conductances from three large-gap PCT tunnel junctions (black curves) obtained near a surface patch that typically displays NbC in the Raman spectrum. Regions ouside the patch display tunneling conductances typical of pure Nb (red curve) which is close to the sub-gap feature seen in the black curves.

References

[1] L. E. Toth, *Transition Metal Carbides and Nitrides* (Academic Press, New York, 1971).

[2] J. Zmuidzinas, Annu. Rev. Condens. Matter Phys. **3**, 169 (2012).

[3] J. A. Klug, N. G. Becker, N. R. Groll, C. Cao, M. S. Weimer, M. J. Pellin, J. F. Zasadzinski, and T. Proslier, Appl. Phys. Lett. **103**, 211602 (2013).

[4] R. Romestain, B. Delaet, P. Renaud-Goud, I. Wang, C. Jorel, J.-C. Villegier, and J.-P. Poizat, New Journal of Physics **6**, 129 (2004).

[5] Z. Wang, D. Liu, S.-L. Li, J. Li, and S.-C. Shi, Supercond. Sci. Technol. **27**, 075003 (2014).

[6] C. M. Varma and W. Weber, Phys. Rev. B **19**, 6142 (1979).

[7] B. M. Klein, L. L. Boyer, and D. A. Papaconstantopoulos, Solid State Commun. **20**, 937 (1976).

[8] D. Reznik, Advances in Condensed Matter Physics **Article ID 523549** (2010).

[9] S. Blackburn, M. Cote, S. Louie, and M. L. Cohen, Phys. Rev. B **84**, 104506 (2011).

[10] E. I. Isaev, S. I. Simak, I. A. Abrikosov, R. Ahuja, Y. K.Vekilov, M. I. Katsnelson, A. I. Lichtenstein, and B. Johansson, J. Appl. Phys. **101**, 123519 (2007).

[11] E. G. Maksimov, M. V. Magnitskaya, S. V. Ebert, and S. Y. Savrasov, JETP Lett. **80** (2004).

[12] Z. P. Yin, A. Kutepov, and G. Kotliar, Phys. Rev. X **3**, 021011 (2013).

[13] H. Wipf, M. V. Klein, and W. S. Williams, Phys. Stat. Sol. (b) **108**, 489 (1981).

[14] M. V. Klein, Phys. Rev. B **24**, 4208 (1981).

[15] M. V. Klein and S. B. Dierker, Phys. Rev. B **29**, 4976 (1984).

[16] Whereas tunneling spectroscopy can measure $\alpha^2F(\omega)$ the two-phonon Raman is roughly proportional to $\alpha^4F(\omega)$, Miles Klein (private communication).

[17] R. Kaiser, W. Spengler, S. Schicktanz, and C. Politis, Phys. Stat. Sol. (b) **87**, 565 (1978).

[18] C. Cao, et al., Phys. Rev. ST Accel. Beams **16** (2013).

[19] A. Romanenko, G. Wu, and L. D. Cooley, in *SRF2011*, Chicago, IL, 2011).

[20] A. Dzyuba and L. D. Cooley, Supercond. Sci. Technol. **27**, 035001 (2014).

[21] P. Maheshwari, F. A. Stevie, G. Myeneni, G. Ciovati, J. M. Rigsbee, and D. P. Griffis, in *FIRST INTERNATIONAL SYMPOSIUM ON THE SUPERCONDUCTING SCIENCE AND TECHNOLOGY OF INGOT NIOBIUM* (AIP Publishing, 2011), Vol. 1352, p. 151.

[22] Z. C. Szkopiak and A. P. Miodownik, J. Nucl. Mater. **17**, 20 (1965).

[23] T. R. Bieler, et al., Phys. Rev. ST Accel. Beams **13**, 031002 (2010).

[24] L. D. Cooley, et al., Ieee T. Appl. Supercon. **21**, 2609 (2010).

[25] M. Uz and R. H. Titran, AIP Conf. Proc. **217**, 172 (1991).

[26] X. Zhao, G. Ciovati, and T. R. Bieler, Phys. Rev. ST Accel. Beams **13**, 124701 (2010).

[27] W. Spengler and R. Kaiser, Solid State Commun. **18**, 881 (1976).

[28] G. K. Tirumalasetty and e. al., Acta Mater. **59**, 7406 (2011).

[29] P. Giannozzi, et al., J. Phys. Condens. Matter **21**, 395502 (2009).

[30] D. Vanderbilt, Phys. Rev. B **41**, R7892 (1990).

[31] S. Baroni, S. D. Gironcoli, A. D. Corso, and P. Giannozzi, Rev. Mod. Phys. **73**, 515 (2001).

[32] J. P. Perdew, K. Burke, and M. Ernzerhof, Phys. Rev. Lett. **77**, 3865 (1996).

[33] G. Kresse and J. Furthmuller, Phys. Rev. B **54**, 11169 (1996).

[34] A. Togo, F. Oba, and I. Tanaka, Phys. Rev. B **78**, 134106 (2008).

[35] L. Ozyuzer, J. F. Zasadzinski, and K. E. Gray, Cryogenics **38**, 911 (1998).

[36] R. Jha and V. P. S. Awana, J. Sup. Nov. Mag. **25**, 1421 (2012).